Proc. Natl. Sci. Counc. ROC(A)
Vol. 24, No. 5, 2000. pp. 341-351

Laminar Separation of Flow Past a Circular Cylinder between Two Parallel Plates

JIAHN-HORNG CHEN

Department of System Engineering and Naval Architecture
National Taiwan Ocean University
Keelung, Taiwan, R.O.C.

(Received November 4, 1999; Accepted January 17, 2000)

ABSTRACT

In the literature, the separation of a uniform flow past a circular cylinder is a classical problem. Traditionally, most studies were conducted in an unbounded flow domain, which introduces insurmountable difficulties into the analysis from the theoretical and numerical points of view. The present study was carried out in domains bounded by two parallel plates, and the effects of three different sets of boundary conditions on the flow development were explored. The first two sets of boundary conditions represent infinite and semi-infinite channel flows disturbed by the presence of a cylinder, respectively. The third one represents a lateral domain truncation usually encountered in computations of external flows. A comparison between these two categories reveals that the specification of boundary conditions does not significantly affect the onset Reynolds number of the recirculating eddy. However, under the third set of boundary conditions, the development of separation bubbles is slightly nonlinearly related to the Reynolds number and the onset separation Reynolds number. In addition, the growth of the separation bubbles varies significantly for different boundary setups and diameter-to-width ratios.

Key Words: laminar separation, boundary conditions

I. Introduction

The study of viscous flow phenomena behind a circular cylinder in an unbounded region has a long history dating back to the nineteenth century. Since then, various important features common to practical flows that are usually complicated geometrically have been observed in this simple flow setup. Therefore, due to its scientific and engineering significance, this flow has motivated numerous scientists and engineers to investigate its flow physics and engineering applications through theoretical, experimental and, more recently, computational approaches.

One of the most fundamental phenomena observed in this flow is laminar separation at low Reynolds numbers. The flow separates on the downstream side of the cylinder at Reynolds numbers greater than some onset value. Separation occurs due to the fact that vorticity convection is more effective than vorticity diffusion. Once separation occurs, two symmetric standing eddies then form and attach to the cylinder. Their size grows as the Reynolds number is increased.

Regarding this phenomenon, there have been many reports in the literature. Most studies have attempted either experimentally or computationally to simulate the unbounded flow in a domain which is bounded in some direction (usually normal to the inflow). A literature survey shows that early pioneering investigations relied mainly on experimental observations, probably due to the lack of an effective analytical tool. Various estimations of the onset Reynolds number beyond which the flow separates from the cylinder have been reported, e.g., 3.2 (based on the diameter of the cylinder and the uniform velocity of the incoming flow) reported by Nisi and Porter (1923), 6 reported by Homann (1936), 5 reported by Taneda (1956), and 4.4 reported by Coutanceau and Bouard (1977). Such variability in experimental findings is somewhat to be expected. It arises partly due to two facts. On the one hand, at the early development stage of the attached eddies, their sizes are quite small. On the other hand, their positions are situated in the immediate neighborhood of the rear stagnation point where the velocity is extremely small. Therefore, they are quite difficult to detect immediately upon their emergence. Nevertheless, Pruppacher *et al*. (1980) summarized various experimental data and concluded that the standing eddy should begin to develop at a Reynolds number of around 5.

One point about the experiments which needs be addressed is that though they attempted to simulate the flow in an unbounded domain, they were carried out in facilities of finite size. Therefore, one must examine how the presence of confining walls affected the development of the flow phenomena. Several reports have focused on this consideration, including works by Grove *et al*. (1965), Acrivos *et al*. (1968) and Coutanceau and Bouard (1977).

In general, all the data in these references show that the onset Reynolds number increases as the diameter-to-width ratio (defined as the ratio of the diameter of the cylinder to the characteristic length of the experimental apparatus) is increased, and that the effect is significant even at a small ratio (say, 0.07). In addition, all these three experiments yielded results which indicated that the eddy length varied nearly linearly with the Reynolds number at a finite diameter-to-width ratio.

As for numerical studies, the problem of estimating the onset Reynolds number for separation has not yet been carefully and systematically investigated, though many reports on computationally separated flow can be found in the literature (see, e.g., Coutanceau and Bouard (1977)). More recently, the most extensive numerical study on standing eddies was done by Fornberg (1980, 1985). He attempted to simulate the unbounded flow in a carefully truncated flow domain. The truncation was based on Oseen approximation and some theoretical considerations. Then he computed the flow within the truncated region at Reynolds numbers up to 600 and studied the eddy development in detail, including the vorticity distribution, length growth rate, and so on. Based on careful computations, he concluded that the eddy region grew in length approximately linearly with the Reynolds number.

As for theoretical investigations, most of the studies have been done by Smith (1979, 1981, 1985). Starting with a triple-deck model, he showed that in an infinite domain, the length of the eddy was of order of Reynolds number. That is, the relation between the length and the Reynolds number is linear. This theoretical conclusion has been confirmed by many experiments and a numerical study by Fornberg (1985). However, Smith's theory is unable to predict the onset Reynolds number since he assumed that the eddy appeared for Reynolds numbers greater than zero.

In the literature, it is quite interesting to find that little attention has been paid to the problem of determining the onset Reynolds number at which twin eddies appear. As mentioned above, determining this number is still beyond the capability of current theoretical development. This remains an open problem requiring further investigation. It was our purpose in the present study to examine computationally the flow at the early separation stage and to determine the onset Reynolds number.

However, instead of considering this in a traditional manner where the flow domain extends to infinity in all directions, we this problem by imposing two parallel plates so that the flow is bounded in some directions. We do so for two reasons. Firstly, for a flow which is unbounded in all directions, truncation of the flow domain is inevitable in any numerical simulation. However, this will pose many difficulties, mainly due to the fact that there are only partial estimates for the decay of solutions of the Navier-Stokes equations at large distances. Accordingly, there is no way of knowing how to truncate the flow domain for computational purposes so as to provide a provable approximation of the flow in the unbounded domain. Secondly, as mentioned above, since all experiments must be carried out in experimental facilities of finite size, no theoretical or computational investigation can be directly compared with experimental investigations. As for the present study under the imposition of two parallel plates, the result can be directly verified or compared with the results of careful experiments.

II. Mathematical Formulation of Flows

A circular cylinder is placed in the flow bounded by two parallel plates which extend upstream and downstream infinitely far, as schematically shown in Fig. 1. The flow is driven by either pressure gradients or plate motions, depending on the specified boundary conditions, which will be prescribed later. A recirculating region of length l is formed for Reynolds numbers exceeding some onset values. The width of the gap between the two plates is w, and the diameter of the cylinder is $d < w$. The center of the cylinder is on the centerline of the flow domain, which forms a symmetric flow.

The fluid motion in the domain can be mathematically represented by the incompressible continuity and momentum equations, which, in nondimensional form, are

$$\nabla \cdot \boldsymbol{U} = 0, \tag{1}$$

$$\boldsymbol{U} \cdot \nabla \boldsymbol{U} = -\nabla p + \frac{1}{R} \nabla^2 \boldsymbol{U}. \tag{2}$$

Here $\boldsymbol{U}(\boldsymbol{x}) = (u(\boldsymbol{x}),v(\boldsymbol{x}))$ and $p(\boldsymbol{x})$ are the velocity and pressure fields, respectively, at a field point $\boldsymbol{x} = (x,y)$ in the flow domain D. R is the Reynolds number, defined as

$$R = \frac{U_c d}{\nu}, \tag{3}$$

where ν is the kinematic viscosity of the fluid and U_c is the far-upstream centerline velocity.

To solve the governing equations, one must implement proper boundary conditions. These conditions can

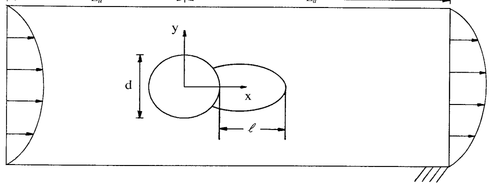

Fig. 1. Schematic of the flow domain.

be set up to represent different flow conditions, depending on what motion of the plates and what upstream fluid flow are prescribed. Three different flows of particular interest are described in the following.

(1) *Flow between two stationary infinite plates*.
This flow is driven by a constant pressure gradient. Without the presence of a cylinder, such a flow is usually referred to as Poiseuille flow. Because of viscous dissipation, the flow far upstream and downstream of the cylinder must be fully developed. Consequently, the boundary conditions are

$$\boldsymbol{U} = \begin{cases} 0, & \text{along the two parallel walls and on the cylinder surface,} \\ (1-4y^2)\boldsymbol{i}, & \text{far upstream and downstream.} \end{cases}$$

The nondimensional volume flow rate per unit width is 2/3.

(2) *Flow between two stationary semi-infinite plates*.
This prescription constitutes an entrance flow between parallel plates. In this situation, the inflow can be readily prescribed with a uniform velocity distribution at the entrance. The cylinder is placed within the uniform core of the entrance flow, which results when the cylinder is not present. Again, due to viscous dissipation, the flow develops downstream, and finally, a fully developed velocity profile is achieved for a low Reynolds-number flow. Therefore, the boundary conditions can be specified as follows:

$$\boldsymbol{U} = \begin{cases} 0, & \text{along the two parallel walls and on the cylinder surface,} \\ \boldsymbol{i}, & \text{at the entrance of the upstream boundary,} \\ (\frac{3}{2}-6y^2)\boldsymbol{i}, & \text{at the far downstream boundary.} \end{cases}$$

The nondimensional volume flow rate for this setup is unity, which is different from that of the first setup.

(3) *Flow between two infinite plates moving at a constant speed*.
In this case, the flow is driven by the motion of the plates. Clearly, the resulting incoming flow is uniform far upstream. This set of boundary conditions represents, in effect, an artifice which truncates an unbounded flow in some directions for computational purposes. It has most often been employed in previous studies to examine numerically the external uniform flow past a circular cylinder. However, a problem associated with this set of conditions is its implication that the vorticity generated by the cylinder cannot diffuse beyond the lateral boundaries. In addition, one of the difficulties which may arise in this setup is that, as far as our understanding of the physics is concerned, there exists no physically sound or mathematically rigorous downstream boundary condition. "Approximate" conditions, in the sense that they may yield "good" approximate solutions to the real physical flow, are usually employed. In this study, we employed the downstream boundary conditions which have most often been used in the literature. All of the boundary conditions are specified as follows:

$$\boldsymbol{U} = \begin{cases} 0, & \text{on the cylinder surface,} \\ \boldsymbol{i}, & \text{along the two parellel walls and at the entrance of the upstream boundary,} \end{cases}$$

and

$$\partial \boldsymbol{U}/\partial x = 0, \quad \text{on the downstream boundary.}$$

The nondimensional flow rate per unit width is unity, which is the same as that under the second set of boundary conditions.

To sum up, one of the advantages of introducing two parallel plates is that one can easily specify physically and mathematically rigorous boundary conditions, as argued by Chen *et al*. (1995). This is especially true for the first two flow setups. In addition, the computational domain is legally bounded in the direction normal to the incoming flow.

In practical computations, we take advantage of the fact that all three flow setups and the flow phenomena which are of interest in the present study are all symmetric about the centerline. This common feature reduces the amount of computation since one can investigate the flow development in only half of the domain and impose symmetric boundary conditions on the centerline, i.e., $\partial u/\partial y = 0$ and $v = 0$, along the centerline.

Finally, imposition of two parallel plates gives rise to a geometrical parameter, namely, the diameter-to-width ratio D_r:

$$D_r = \frac{d}{w}. \tag{4}$$

This parameter serves as an indicator that shows how "broad" the flow extends in the lateral direction.

III. Numerical Solution Formulation

The penalty Galerkin weak formulation was employed to formulate the variation form of the Navier-Stokes equations, and the resulting equations were discretized using the Crouzeix-Raviart finite element method (Crouzeix and Raviart, 1973). The particular approach used in the present study was to employ enriched $P_2^+ - P_1$ elements.

In the penalty methods, a perturbation consisting of the product of a small parameter and the pressure is introduced to the continuity equation. Therefore, instead of solving the exact differential equation system, Eqs. (1) and (2), one solves the following perturbed Navier-Stokes equations:

$$\boldsymbol{U} \cdot \nabla \boldsymbol{U} = -\nabla p + \frac{1}{R} \nabla^2 \boldsymbol{U}, \tag{5}$$

$$\nabla \cdot \boldsymbol{U} = -\varepsilon p. \tag{6}$$

The feasibility of this approach has been demonstrated by Temam (1979).

Then, the perturbed governing equations can be formulated variationally as follows:

$$a(\boldsymbol{U},\boldsymbol{v}) + \frac{1}{\varepsilon}(\nabla \cdot \boldsymbol{U}, \nabla \cdot \boldsymbol{v}) + c(\boldsymbol{U},\boldsymbol{U},\boldsymbol{v}) = 0, \tag{7}$$

where $\boldsymbol{v} = \boldsymbol{v}(\boldsymbol{x})$ is any eligible test vector-valued function satisfying appropriate boundary conditions. Each term in Eq. (7) is defined as follows:

$$a(\boldsymbol{u},\boldsymbol{v}) = \int_D (\nabla \boldsymbol{u} : \nabla \boldsymbol{v}) d\boldsymbol{x}, \tag{8}$$

$$c(\boldsymbol{u},\boldsymbol{v},\boldsymbol{w}) = R \int_D \left[(\boldsymbol{u} \cdot \nabla) \boldsymbol{v} \right] \boldsymbol{w} d\boldsymbol{x}, \tag{9}$$

and $(\cdot, \cdot)$ is the usual inner product defined as $(r(\boldsymbol{x}), s(\boldsymbol{x})) = \int_D r(\boldsymbol{x}) s(\boldsymbol{x}) dx$. In Eq. (8),

$$\nabla \boldsymbol{u} : \nabla \boldsymbol{v} = \frac{\partial u_1}{\partial x}\frac{\partial v_1}{\partial x} + \frac{\partial u_1}{\partial y}\frac{\partial v_1}{\partial y} + \frac{\partial u_2}{\partial x}\frac{\partial v_2}{\partial x} + \frac{\partial u_2}{\partial y}\frac{\partial v_2}{\partial y},$$

with $\boldsymbol{u} = (u_1, u_2)$ and $\boldsymbol{v} = (v_1, v_2)$. Once the velocity field is solved, the pressure field can be directly recovered from Eq. (6).

1. Computation Procedures

After the Galerkin weak formulation, Eq. (7), is established, the approximate problem from which the finite element solution is determined is defined in the usual manner. In the present study, the Crouzeix-Raviart quadratic finite element method was employed. The main advantage of this penalty method lies in the fact that the computation of the velocity and that of the pressure can be decoupled, which leads to smaller systems of equations with fewer unknowns. In addition, no partial pivoting is needed to solve the associated linear equation system. Nevertheless, in practical computations, the value of the penalty parameter ε must be chosen carefully. The parameter must be small enough to approximate the incompressible continuity equation well and yet large enough to prevent the resulting simultaneous equation system from becoming so numerically illconditioned that it cannot be solved in matrix computations. Throughout the present study, ε was set to a value of 10^{-6}, which produced a fairly consistent, good quality numerical results.

The application of the Galerkin finite element procedure to the steady perturbed Navier-Stokes equations results in a set of nonlinear algebraic equations that may be represented in matrix form as

$$\boldsymbol{A}(\boldsymbol{U})\boldsymbol{U} = \boldsymbol{B}, \tag{10}$$

where $\boldsymbol{A}$ is the global system matrix, $\boldsymbol{U}$ the discretized velocity field, and $\boldsymbol{B}$ a vector which includes effects due to boundary conditions.

To solve the nonlinear equation system, an iterative solution method must be chosen. Here, the method of fixed point iteration (Picard iteration) was used for the first several iterations, and then a quasi-Newton method was employed to accelerate the convergence of iterations. This strategy was adopted because the former method converges for a fair range of Reynolds numbers and initial guesses (though its convergence rate is only asymptotically linear), and the latter method is computationally economic since its convergence rate is almost asymptotically quadratic (though its radius of convergence is sometimes quite small).

The algorithm for the fixed point iteration may be written as

$$\boldsymbol{A}(\boldsymbol{U}_i)\boldsymbol{U}_{i+1} = \boldsymbol{B}, \quad \text{for } i = 1, 2, 3, \cdots, \tag{11}$$

where the subscript i denotes the i-th iteration and $\boldsymbol{U}_1$ is some initial guess. For the quasi-Newton method, the algorithm is formally written as

$$\boldsymbol{U}_{i+1} = \boldsymbol{U}_i - s\boldsymbol{J}^{-1}\boldsymbol{R}_i, \tag{12}$$

where s is the relaxation factor, $\boldsymbol{J}$ the Jacobian matrix, and $\boldsymbol{R} = \boldsymbol{R}(\boldsymbol{U}_i)$ the residual, defined as

$$\boldsymbol{R}(\boldsymbol{U}) = \boldsymbol{A}(\boldsymbol{U})\boldsymbol{U} - \boldsymbol{B}.$$

For the purpose of economy, the Jacobian matrix is updated by means of a first-order direct inverse approximation proposed by Broyden (1965).

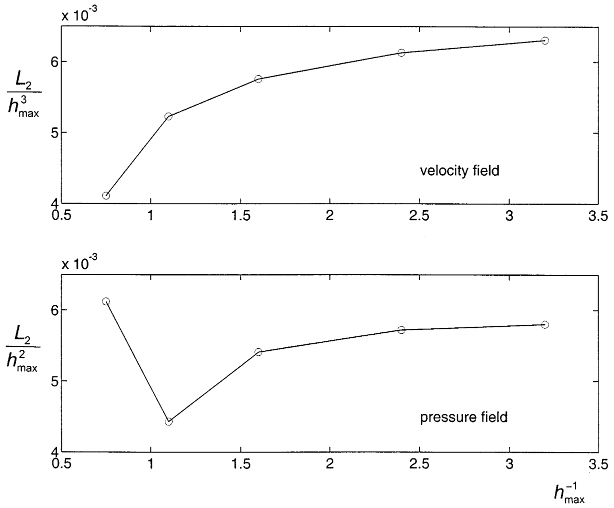

Fig. 2. Convergence tests of the current finite element scheme.

2. Computational Considerations

Before any meaningful solution could be achieved, several aspects of the computations had to be first addressed.

First of all, we carried out a series of computations to assess the convergence of solutions based on mesh refinement. Several globally similar meshes with different degrees of refinement were generated on the same domain, $(x,y) \in [-3.0, 4.0] \times [-0.5, 0.5]$. The ratios of the total grid numbers in the computational domain, from the coarsest to the finest one, were approximately 1.0 : 2.25 : 4.0 : 9.0 : 16.0 : 36.0. The coarsest triangulation consisted of 252 triangles and 817 nodal points while the finest mesh was comprised of 9360 triangles and 28,445 nodal points. In these tests, the flow at $R = 1$ and $D_r = 0.6$ was computed, under the first type of boundary conditions. The penalty parameter was set between 10^{-6} and 10^{-9}, depending on the refinement of the mesh.

Assuming that the solution which is obtained with the most refined mesh represents the "exact" solution, one can calculate the measure of the relative velocity L_2 difference between the two solutions. Define

$$L_2 = \frac{\sum_{i=1}^{N}\sum_{j=1}^{M} A_i \left|(\boldsymbol{U}_f)_{ij} - (\boldsymbol{U}_c)_{ij}\right|^2}{\sum_{i=1}^{N}\sum_{j=1}^{M} A_i \left|(\boldsymbol{U}_f)_{ij}\right|^2},$$

where N denotes the number of triangles in a particular discretization, M the number of nodes on each triangle, and A_i the area of the i-th triangle. The subscripts f and c represent the finest mesh and any coarser meshes, respectively. In addition, $|\cdot|$ denotes the magnitude of a vector quantity. The L_2 difference for the pressure field is similarly defined. In order to characterize the degree of refinement of each mesh, the length of the longest triangle edge in a triangulation, denoted by $h_{\max}$, was chosen as the length scale to represent the size of the mesh. The results shown in Fig. 2 indicate that the orders of convergence for the velocity and pressure approximations due to mesh refinement approaches the respective theoretical value, 3 for the velocity field and 2 for the pressure field.

As for the second aspect, of the computations, we found that the size of the cylinder relative to the width of the gap between the two parallel plates played an important role in generating proper meshes for computations. Different strategies for mesh generation in the region near the cylinder must be developed for different diameter-to-width ratios in order to not severely distort the meshes, which would lead to "bad" solutions. Shown in Figs. 3–5 are three different triangulations in the region around the cylinder. They were employed for small, medium, and

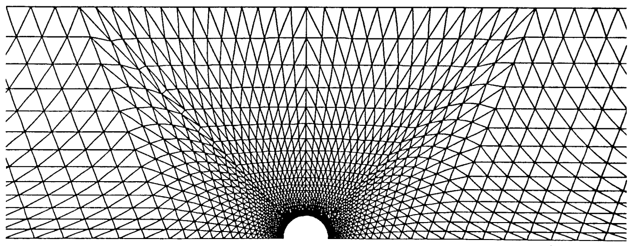

Fig. 3. Domain triangulation near the cylinder for $D_r \le 0.2$.

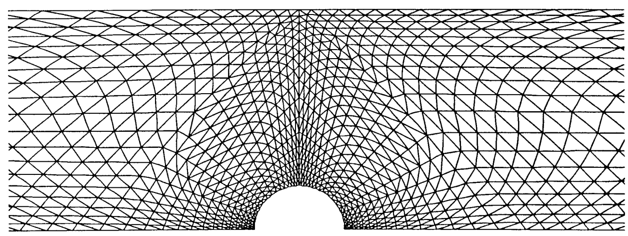

Fig. 4. Domain triangulation near the cylinder for $0.2 < D_r \le 0.7$.

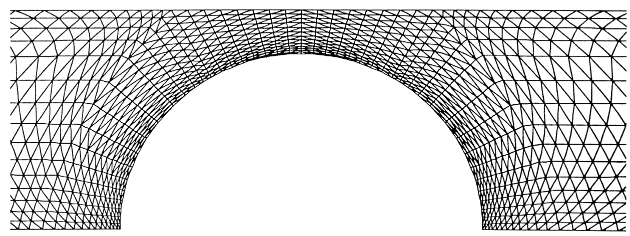

Fig. 5. Domain triangulation near the cylinder for $D_r > 0.7$.

large diameter-to-width ratios, respectively. For $D_r \leq 0.2$, the triangulation shown in Fig. 3 was used. In this range, the cylinder is rather small, compared to the width between the parallel plates, and the eddy region is also quite small. Therefore, a very fine mesh must be employed around the cylinder, especially in the expected eddy region, in order to obtain an accurate description of the eddies. Figure 4 shows the triangulation for intermediate diameter-to-width ratios ($0.2 < D_r \leq 0.7$). It turned out that computations in this range were easiest. When D_r exceeds 0.7, this type of triangulation is no longer appropriate because it becomes severely distorted near the constriction. Instead, the triangulation shown in Fig. 5 is a more suitable one.

The third aspect which had to be considered with regard to the computations was how to determine the onset Reynolds number at which the flow separates from the cylinder. Generally speaking, it is quite difficult to determine through computations the onset Reynolds number directly since a very fine mesh would be required to detect the emergence of eddies. Therefore, an indirect extrapolation procedure was instead employed to estimate the value of the onset Reynolds number. The physical property adopted for the extrapolation procedure was the eddy length because we found that it was related to the Reynolds number through a simple relation. The procedure is briefly described as follows.

For each diameter-to-width ratio, the flow field was computed at several Reynolds numbers. The computed centerline velocity distribution was then examined, and the point where $u = 0$ was located and was defined as the end of the eddy region. To determine the location of this point, a quadratic interpolation procedure using the velocity data found computationally was employed. This procedure is feasible because the shape function in enriched $P_2^+ - P_1$ Crouzeix-Raviart elements is itself quadratic for the velocity field. Through this procedure, a curve of the eddy length versus the Reynolds number was drawn, and an extrapolation of the curve fitted by an appropriate polynomial function was made to estimate the onset Reynolds number.

Finally, truncation of the domain had to be considered in the streamwise direction. We would expect that the extent of computational domain should be carefully chosen in order for the flow phenomenon near the cylinder to not be distorted. To accomplish this, we usually truncated the domain at several different upstream and downstream locations and examined the effects due to truncation on the flow development behind the cylinder, especially the global structure of the twin eddies. This procedure had to be first carried out for every diameter-to-width ratio of interest to ensure that a domain-truncation independent solution could be obtained in the region behind the cylinder.

A thorough study showed that for each of the three types of flow setup, the eddy length could be accurately obtained as long as the domain was "long" in the sense that the domain could accommodate the development of the closed recirculating flow. Figure 6 shows a typical development of centerline velocity distributions for different truncations. These results were obtained under the conditions $D_r = 0.2$ and $R = 24$. Both plates were fixed (i.e., the first set of boundary conditions). The downstream truncated boundary was set to be twice as far away from the center of the cylinder as the upstream one. The computational results seemed to indicate that the flow development strongly depended on the domain truncation, unless the domain was long enough for "natural" development. For a short truncation, the flow was forced to develop in the truncated region, and a fully developed flow was forced to develop on the boundary. However, it was also noted the eddy length seemed to not be strongly influenced by the computational domain. As shown in Table 1 for the computed eddy length at different truncations, even for a very short truncation, the eddy length was accurate up to the third decimal. Similar results were also obtained for both of the other sets of boundary conditions.

To summarize, the results of the domain-truncation study seem to provide with us a good property which enables us to conduct computations in a small truncated domain which would, in turn, reduce the computation time.

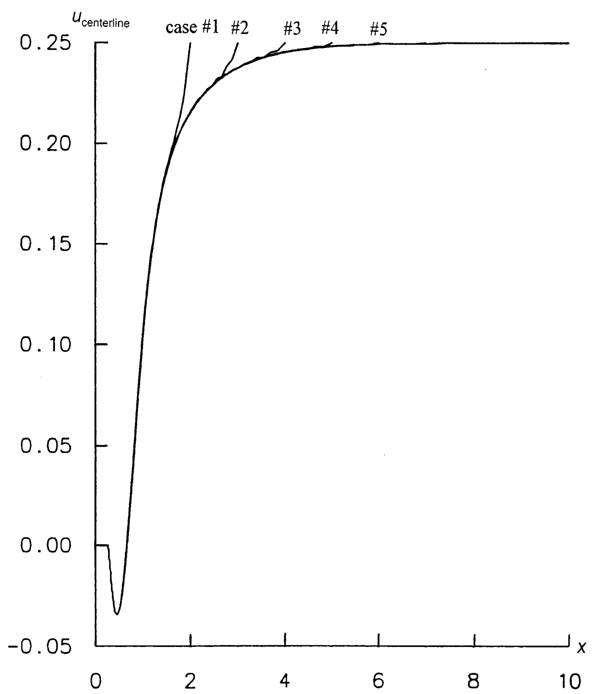

Fig. 6. Effect of the domain length on the centerline velocity distribution at $D_r = 0.2$ and $R = 24$ under the first type of boundary data.

Table 1. Computed Eddy Length for Different Upstream and Downstream Truncations for the First Flow Setup (D_r = 0.2 and R = 24)

Case #	L_u	L_d	L_{eddy}
1	1.0	2.0	0.4123
2	1.5	3.0	0.4121
3	2.0	4.0	0.4122
4	2.5	5.0	0.4121
5	3.0	6.0	0.4121
6	3.5	7.0	0.4121
7	4.0	8.0	0.4121
8	4.5	9.0	0.4121
9	5.0	10.0	0.4121

IV. Results and Discussion

General computations showed that care must be exercised in predicting small recirculating regions which might appear under either small diameter-to-width ratios or Reynolds numbers slightly above the separation onset value. The mesh in the wake region must be fine enough to accurately capture the small flow region.

A measure of the mesh size can be properly defined as

$$H = \frac{h_{\max}}{\sqrt{L \cdot w}},$$

where $L = L_u + L_d$ is the length of the truncated domain in the streamwise direction. Since, in the following computations, all the meshes employed for each particular value of D_r are similar in the sense that a finer mesh is obtained by uniformly refining a coarser one, the value of H is an indicator which can properly show the influence of the mesh size on the variation of the solution.

For the first set of boundary conditions (Poiseuille flow far upstream and downstream), a typical computed result is shown in Fig. 7. The corresponding D_r = 0.1, L_u = 1.0 and L_d = 2.0.

One of the most significant features is that as the mesh was refined, the computed data conformed very closely to a linear relation between the eddy length and the Reynolds number. In fact, through a linear least-squares fitting procedure, it was found that all these data could be well fitted by a straight line like the solid one shown in Fig. 7. This observation indicates that it is quite possible to easily and reliably estimate the onset Reynolds number by using a linear extrapolation procedure. For D_r = 0.1, the extrapolation result shows that the onset Reynolds number was R_{onset} = 6.9.

As an independent check of the estimate of R_{onset}, a lower bound was also determined through computation at a Reynolds number smaller than the estimated R_{onset}. For the case shown in Fig. 7, we arbitrarily chose a Reynolds number of 6.7 for verification purposes. The computation was carried out under a very fine mesh with the same L_u and L_u shown above and with H = 0.0462. This triangular mesh was four times as dense as the finest one employed in the computations used to find the onset Reynolds number shown in Fig. 7. The computational result did show that there was no recirculating region attached to the cylinder. Therefore, this seemed to confirm that the onset Reynolds number was not smaller than 6.7.

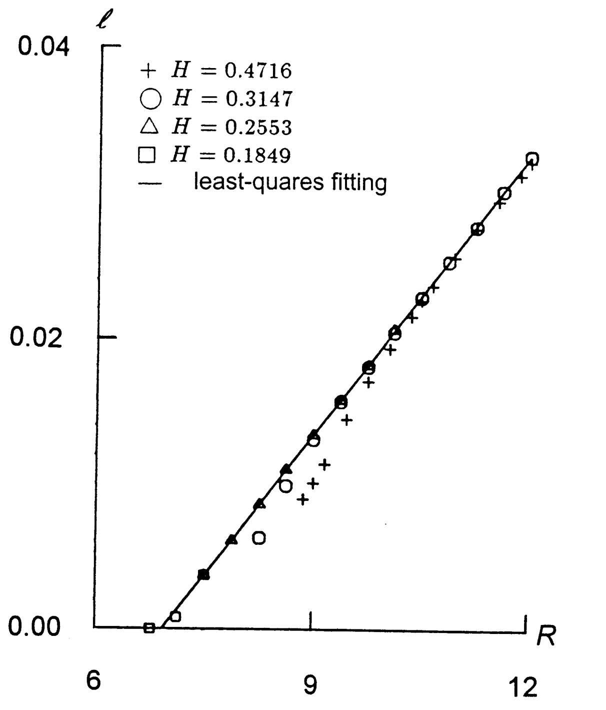

Fig. 7. Computed eddy lengths at various Reynolds numbers under the first set of boundary conditions (D_r = 0.1).

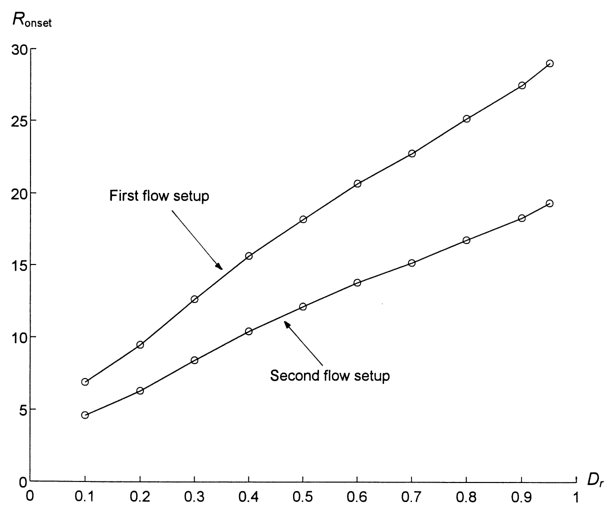

Fig. 8. The onset Reynolds number at various diameter-to-length ratios for the first and second flow setups.

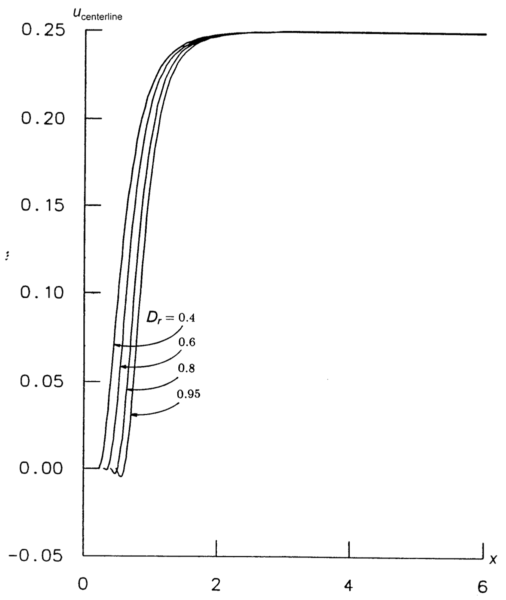

Fig. 9. Centerline velocity recovery after the flow passes the cylinder under the first type of boundary data.

The onset Reynolds numbers of flow separation for other diameter-to-width ratios are shown in Fig. 8. The value of R_{onset} increased as the diameter-to-width ratio was increased. To summarize the results of many experimental studies available in the literature, it is generally believed that the possible onset Reynolds number in an unbounded domain with a uniform incoming flow lies between four and six. According to the trend of the present computational results, the curve seems to converge to the same range as D_r approaches zero. However, the function between the onset Reynolds number and the diameter-to-length ratio seems to not be very straightforward; no extrapolation estimate of the onset Reynolds number at D_r = 0 was attempted.

In addition, the present computations show that although the flow perturbation due to the presence of the cylinder varied in magnitude for different diameter-to-width ratios, the decay of the disturbances in the downstream flow was only slightly affected for a fixed Reynolds number based on the width of the gap between the two plates. As an example, Fig. 9 shows the recovery velocity distribution on the centerline for various diameter-to-width ratios at R = 75. It is clear that each distribution reaches its unperturbed value at about the same distance away from the cylinder. In fact, this phenomenon can be understood since the decay rate is determined by the eigenvalues of the spatial stability analysis of the plane Poiseuille flow, which is independent of the size of the cylinder.

For the second type of flow setup (entrance flow at the upstream boundary), the flow field could be computed in a way similar to that done for the flow with the first type of boundary conditions. We first compared the centerline velocity distributions (a feature of the development of the recirculating region) in the flow fields obtained using these two sets of boundary data. However, to make a meaningful comparison, we had to define a new Reynolds number.

There are two reasons for defining a new Reynolds number. First, based on the present definition, the two different sets of boundary conditions result in flows with different volume flow rates at the same Reynolds number or, equivalently, the same centerline velocity provided that the diameter of the cylinder stays the same. This, in turn, results in different mean velocities and, therefore, may affect the development of the recirculating region behind the cylinder. For comparison purposes, a new Reynolds number based on the average velocity at the narrowest section of passage, i.e.,

$$R_{\text{ave}} = \frac{(U_{\text{ave}})_{x=0}\, d}{\nu},$$

was defined, and it seems more suitable to describe the flow phenomena appearing behind the cylinder. This definition takes the volume flow rate into consideration for the flow development behind the cylinder.

Based on this new definition of the Reynolds number, a typical comparison of the centerline velocity distri-

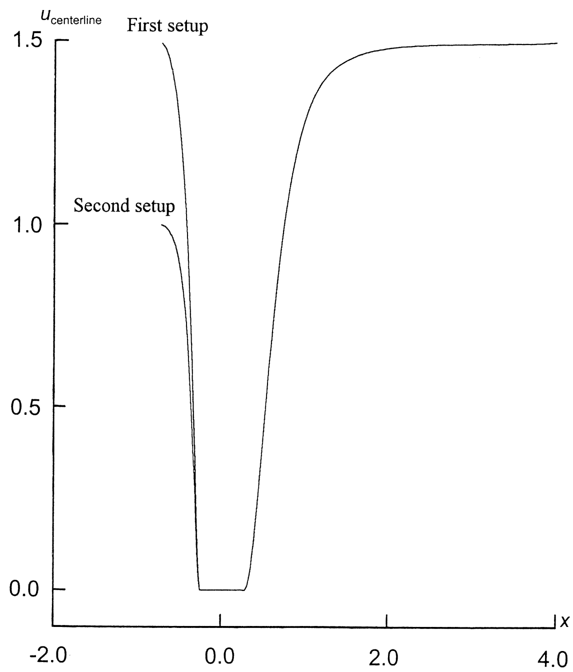

Fig. 10. Comparison of centerline velocity distributions due to different upstream velocity profiles at the inlet boundary (D_r = 0.5 and R_{ave} =160).

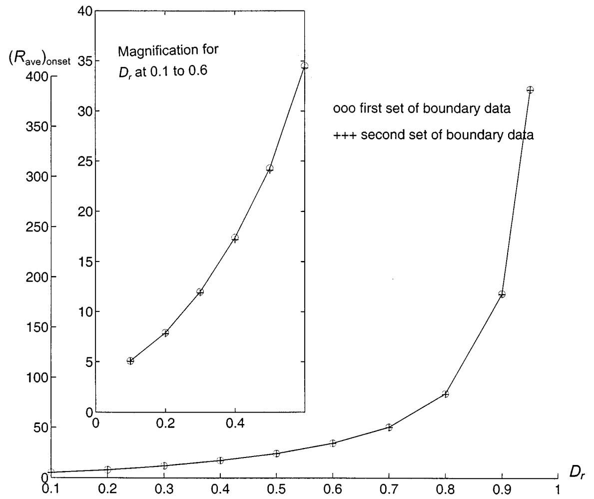

Fig. 11. The onset Reynolds number at various diameter-to-length ratios for the second flow setup.

butions for the two flows at the same R_{ave} is shown in Fig. 10. The computations were carried out under the conditions $D_r = 0.5$, $L_u = 0.7$, $L_d = 4.0$ and $R_{ave} = 80$. It is surprising to observe that the distributions behind the cylinder are so close to each other that it is difficult to tell them apart. This observation leads us to the second reason why the new Reynolds number R_{ave} was thus defined. The characteristic of the flow behind the cylinder seems to indicate that the upstream boundary velocity profiles do not sensitively affect the centerline velocity distribution behind the cylinder or, more precisely, the length of the recirculating region due to flow separation. This could be due to the fact that at a small Reynolds number, viscous effects over the cylinder are prominent. Furthermore, when the flow passes through the narrow passage between the plate and the cylinder, the upstream flow structure may possibly by partially destroyed. Therefore, the effects of different upstream velocity distributions become insignificant for a fixed volume flow rate. In other words, the centerline velocity at the upstream boundary cannot fully reflect the development downstream of the cylinder. As far as the development of the recirculating region is concerned, R_{ave} can serve as a better nondimensional parameter. This point will be made clear in the following discussion.

Similar to the computation for the first flow setup, we also attempted to estimate the onset Reynolds number at various values of D_r via the linear extrapolation procedure used above. Careful computations did show that the relation between the eddy length and the Reynolds number was linear. Therefore, a linear extrapolation seemed feasible for estimating the onset Reynolds number. The results are shown in Fig. 8.

Comparing the trend of the present results with that obtained under the first set of boundary conditions, we observe that there exists some similarity between them as shown in Fig. 8. According to the arguments discussed above, the Reynolds number R based on the centerline velocity at the upstream boundary is not a proper physical parameter for the flow separation and the eddy-forming feature. If we redraw the relation shown in Fig. 8 based on R_{ave}, then we find that the two lines almost coincide with each other, as shown in Fig. 11. This coincidence clearly indicates that the upstream boundary conditions do not play a key role in the development of the flow separation at low Reynolds numbers.

Finally, we studied the third flow setup (effectively, the truncation of an infinite flow in all directions). The computations showed a story different from the otehr two. Two features were observed.

At $D_r = 0.1$, the relation between the eddy length and the Reynolds number was found to be linear, as in the first two flow boundary setups. However, for $D_r > 0.1$, this linear relation was destroyed and became slightly nonlinear. Shown in Fig. 12 are some data computed at $D_r = 0.7$. The curves are slightly concave upward. Computations showed that the nonlinearity of the relation became stronger as D_r was increased. Nevertheless, its effect was quite limited even at a large value of D_r, say 0.7. This phenomenon may be due to somewhat less efficient vorticity diffusion or somewhat faster vorticity convection in the flow field.

Through a careful study of least-squares curve fitting, we found that these data could be well fitted by a quadratic polynomial function, with residuals of less than 10^{-5}. We then used this quadratic relation to extrapolate

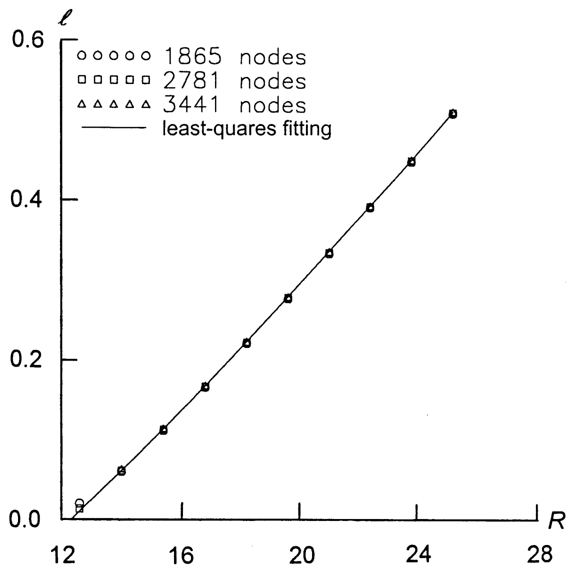

Fig. 12. Computed eddy lengths under various Reynolds numbers (D_r = 0.7).

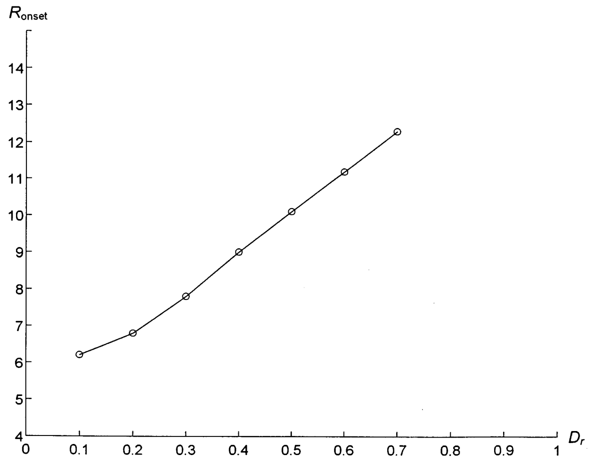

Fig. 13. The onset Reynolds number under various diameter-to-length ratios for the third flow setup.

the onset Reynolds number. The results are shown in Fig. 13.

In addition to the nonlinear growth, we found that at $D_r = 0.1$, the onset Reynolds numbers were 4.6 and 6.2 for the flows, respectively, obtained under the second and third sets of boundary conditions, both of which had the same volume flow rate at the same Reynolds number. This comparison shows that the appearance of separation of the flow with the third boundary data set exhibited significant delay. This delay could also be observed at all other values of D_r as shown in Figs. 8 and 13, but the deviation between them did not vary significantly with D_r.

V. Concluding Remarks

In this study, we have re-examined the development of an attached recirculating eddy behind a cylinder. Our approach is based on introduction of two parallel plates in the streamwise direction. Flows due to different boundary conditions were computed and the results have been discussed. It seems to us that the first two different sets of boundary data (Poiseuille flow past a circular cylinder and entrance flow past a circular cylinder, respectively) did not have significantly different effects on the development of the recirculating flow region and the emergence of flow separation at low Reynolds numbers. They yielded almost the same results under some proper scaling. The elongation development of the recirculating region linearly followed the Reynolds number, however it was defined. This trend is identical to the theoretical arguments put forward by Smith (1979).

The third setup of boundary conditions, which represents the traditional approach, showed a slightly nonlinear relation between the length development of the recirculating region and the Reynolds number in a severely laterally truncated domain, in contrast to the familiar linear relation in an external flow. Furthermore, the onset Reynolds number obtained in this boundary data set showed significant deviation from those obtained under the first two sets. This implies that different boundary data can introduce different vorticity convection and diffusion speeds.

References

Acrivos, A., L. G. Leal, D. D. Snowden, and F. Pan (1968) Further experiments on steady separated flow past bluff objects. *Journal of Fluid Mechanics*, **34**, 25-48.

Broyden, C. G. (1965) A class of methods for solving nonlinear simultaneous equations. *Mathematics of Computation*, **19**, 577-593.

Chen, J. H., W. G. Pritchard, and S. J. Tavener (1995) Bifurcation for flow past a cylinder between parallel planes. *Journal of Fluid Mechanics*, **284**, 23-41.

Coutanceau, M. and R. Bouard (1977) Experimental determination of the main features of the viscous flow in the wake of a circular cylinder in uniform translation. Part 1. Steady flow. *Journal of Fluid Mechanics*, **79**, 231-256.

Crouzeix, M. and P. A. Raviart (1973) Conforming and non-conforming finite element methods for solving the stationary stokes equations. *R. A. I. R. O.*, **R-3**, 33-76.

Fornberg, B. (1980) A numerical study of steady viscous flow past a circular cylinder. *Journal of Fluid Mechanics*, **98**, 819-855.

Fornberg, B. (1985) Steady viscous flow past a circular cylinder up to Reynolds number 600. *Journal of Computational Physics*, **61**, 297-320.

Grove, A. S., F. M. Shair, E. E. Petersen, and A. Acrivos (1965) An experimental investigation of the steady separated flow past a circular cylinder. *Journal of Fluid Mechanics*, **19**, 60-80.

Homann, F. (1936) Der Einfluss grosser Zahigkeit bei der Stromung um den Zylinder und um die Kugel. *Zeitschrift fur Angewandte Mathematik und Mechanik*, **16**, 153-165.

Nisi, H. and A. W. Porter (1923) On eddies in air. *Philosophical Magazine*, **46**, 754-761.

Pruppacher, H. R., B. P. Le Clair, and A. E. Hamielec (1980) Some relations between drag and flow pattern of viscous flow past a sphere and a cylinder at low and intermediate Reynolds numbers. *Journal of Fluid Mechanics*, **44**, 781-790.

Smith, F. T. (1979) Laminar flow of an incompressible fluid past a bluff body: the separation, reattachment, eddy properties and drag. *Journal of Fluid Mechanics*, **92**, 171-205.

Smith, F. T. (1981) Comparisons and comments concerning recent calculations for flow past a circular cylinder. *Journal of Fluid Mechanics*, **113**, 407-410.

Smith, F. T. (1985) A structure for laminar flow past a bluff body at high Reynolds number. *Journal of Fluid Mechanics*, **171**, 263-287.

Taneda, S. (1956) Experimental investigation of the wakes behind cylinders and plates at low Reynolds numbers. *Journal of the Physical Society of Japan*, **11**, 302-307.

Temam, R. (1979) *Navier-Stokes Equations, Theory and Numerical Analysis*, Revised Edition. North Holland, New York, NY, U.S.A.

兩平行無窮平板流場的圓柱剝離流

陳建宏

國立臺灣海洋大學系統工程暨造船學系

摘　要

本文旨在採取一個新的角度，來探討二維流場通過圓柱時所造成的剝離效應。傳統上，這個現象大多在無限流場的架構下來分析，但這在理論上、或是計算上，都造成難以克服的困難，原因之一乃是下游的邊界條件無從界定。在本報告中，我們把流場侷限在兩平板之間，並設定三組不同的邊界條件，來探討流場的發展。第一組邊界條件相當於是無窮平行板間的流場，而第二組是相當於半無窮平行板間的流場，至於第三組則代表一般外流場的計算領域效應。計算結果顯示，在適當的無因次化下，第一組與第二組所造成的效應可說是一致的，而第三組的效應則有些微的非線性現象存在，但不論是那一組邊界條件，對起始的剝離雷諾數都沒有太明顯的影響。此外，不同的封阻程度，對流場與剝離現象的發展，也會帶來相當程度的影響。